Research Square

Preprints are preliminary reports that have not undergone peer review.
They should not be considered conclusive, used to inform clinical practice,
or referenced by the media as validated information.

500 years of May temperature variability in Balochistan reconstructed from Juniperus excelsa tree rings: heat stress, growth-collapse extremes, and implications for an endangered relict forest

Mehvish Majeed

mmajeed@unr.edu

University of Nevada Reno https://orcid.org/0000-0002-5764-6369

Brekhna Gul

University of Swat

Sher Shah

University of Swat

Hamid Ur Rahman

University of Swat

Afaq Ahmad

University of Swat

Maaz Ali

University of Swat

Eman Majeed

Western Caspian University

Sohaib Muhammad

GC University Lahore: Government College University Lahore

Zahid Rauf

Pakistan Forest Institute

Sajjad Saeed

Pakistan Forest Institute

Nasrullah Khan Mandokhel

University of Swat

Research Article

Keywords: dendroclimatology, Juniperus excelsa, Ziarat, temperature reconstruction, Little Ice Age, pointer year analysis, Balochistan, heat stress, Pakistan

Posted Date: November 2nd, 2026

DOI: https://doi.org/10.21203/rs.3.rs-10746072/v1

License: This work is licensed under a Creative Commons Attribution 4.0 International License.
Read Full License

Abstract

The Ziarat juniper forest of Balochistan, Pakistan—among the oldest juniper woodlands documented in the Hindu Kush–Himalayan (HKH) system—provides a valuable proxy archive for reconstructing pre-instrumental climate variability in this data-sparse western arid zone. Using 101 ring-width series from high-elevation *Juniperus excelsa*, spanning 1523–2023 CE, we developed a master chronology (EPS = 0.971; SNR = 33.4) restricted for robust climate interpretation to the post-1700 CE window, where sample depth exceeds the 10–15 series threshold required for EPS ≥ 0.85 (Wigley et al., 1984). A 14-month climate-growth correlation analysis identifies current-year May mean temperature as the single strongest and most coherent driver of radial growth ($r = -0.66$, $p < 0.001$), providing both a statistical and physiological basis for selecting May as the reconstruction target. May mean temperature was reconstructed back to 1523 CE via a calibrated Simple Linear Regression model validated with Leave-One-Out (LOO) cross-validation ($R^2 = 0.43$; $r = 0.66$; RE = 0.51; RMSE = 1.56°C; $p < 0.001$), with robust climatic interpretation confined to the post-1700 CE period and the pre-1700 CE interval treated explicitly as exploratory (EPS < 0.85; Supplementary Fig. S3). Over the robust period, the reconstruction reveals a secondary warm phase during 1700–1770 CE, renewed cooling through much of the eighteenth and nineteenth centuries consistent with Little Ice Age and Dalton Minimum forcing, and a modern warming trend accelerating after ca. 1980 CE that reaches the highest sustained 30-year values in the robust record. Pointer Year Analysis, using a > 70% synchronous growth-collapse threshold applied consistently across the full chronology, identified thirteen extreme events, with the most severe collapses occurring in 1767, 1761, 1801, 1910, and 2010 CE—several of which align temporally with documented regional famines, Dalton Minimum forcing, and monsoon failures, though we treat these as temporal correspondences rather than demonstrated causal links. A 31-year moving correlation analysis shows that the negative temperature-growth relationship strengthened progressively after ca. 1985 CE (r approaching −0.6 to −0.66 for May mean temperature), consistent with, but not conclusive proof of, a warming-driven physiological threshold response that we discuss alongside the alternative and non-exclusive possibility of compounding anthropogenic disturbance (grazing, fuelwood extraction). These results provide the first multi-century climate reconstruction from the Ziarat ecosystem and a quantitative, appropriately bounded baseline for evaluating this critically endangered forest's vulnerability to continued warming.

1. Introduction

The western arid zone of Pakistan—encompassing Balochistan and the interfluves of the Indus and Helmand river systems—is among the most climate-vulnerable regions in South Asia. Observed warming rates in this region have outpaced global means in recent decades, while precipitation trends are characterized by high interannual variability and a declining monsoon signal at lower elevations (Rafiq et al., 2023; Krishnan et al., 2019). Understanding how this region has varied climatically over centennial timescales is essential for contextualizing current warming within a longer-term framework. But instrumental records rarely extend beyond the mid-twentieth century, and paleoclimate proxy data remain sparse.

The Ziarat juniper forest of northern Balochistan represents one of the largest and oldest extant woodland ecosystems dominated by *Juniperus excelsa* (Greek juniper). Individual trees at Ziarat have been dated to more than 5,000 years, making this potentially one of the longest-lived conifer populations on Earth (Sarangzai & Ahmed, 2011). The forest is listed as a UNESCO World Heritage Site candidate and is critically threatened by overgrazing, fuelwood extraction, climate warming, and recurring drought (Ahmed et al., 2006; Jallat et al., 2021). Despite its ecological significance and extraordinary longevity, the dendroclimatic potential of the Ziarat *J. excelsa* population has been only partially explored, and no reconstruction of pre-instrumental climate variability extending beyond the twentieth century has been published from this site (Esper 2000; Esper et al. 2002, 2007; Treydte et al. 2006; Zafar et al. 2016; Asad et al. 2017; Khan et al. 2021; Zhu et al. 2021; Huang et al. 2022; Ahmed et al., 2011; Sarangzai et al., 2012). Existing HKH dendroclimatic reconstructions are concentrated in the northern Karakoram and western Himalayan ranges—e.g., the Karakoram rainfall reconstruction of Khan et al. (2020) and the western Himalayan summer-temperature reconstructions of Khan et al. (2021) and Asad et al. (2023)—all of which sample mesic, monsoon-influenced conifer populations (*Cedrus deodara*, *Pinus wallichiana*) in which growth is primarily precipitation-limited. Ziarat, by contrast, lies at the arid, north-western margin of the South Asian Summer Monsoon where growth is temperature- rather than precipitation-limited. The present chronology therefore does not simply extend an established regional network geographically; it adds a climatically and mechanistically distinct arid-zone node against which the moisture-driven signals of existing HKH reconstructions can be contrasted, and it is, to our knowledge, the first multi-century, absolutely dated climate reconstruction from the Balochistan plateau specifically.

Juniperus species are established dendrochronological proxies across the Hindu Kush–Karakoram–Himalayan (HKH) region and the broader Central Asian arid zone. Their slow radial growth, dense wood anatomy, and strong climate sensitivity make them particularly suitable for high-resolution proxy reconstruction (Treydte et al., 2006; Borgaonkar et al., 2009; Bräuning & Mantwill, 2004). In Pakistan, previous dendroclimatic work with junipers has concentrated on the Karakoram and Hindukush ranges in the north (Ahmed et al., 2011; Khan et al., 2020), leaving the Balochistan plateau—geographically and climatically distinct as a low-latitude, continental-arid environment—almost entirely unrepresented in the regional dendroclimatic network.

The primary climatic limitation at Ziarat has been attributed to summer heat stress rather than precipitation deficit per se, a mechanistic distinction with important ecophysiological implications (Sarangzai & Ahmed, 2011; Ahmed et al., 2006). High May–August temperatures promote stomatal closure, reduce photosynthetic carbon gain, and deplete non-structural carbohydrate reserves needed for late-season xylem formation, effectively coupling tree growth to thermal variability at monthly resolution (Camarero et al., 2018; Anderegg et al., 2020). Understanding whether this heat-stress regime is intensifying under recent warming—and when it may have exceeded historical bounds—is therefore a conservation priority.

This study addresses these knowledge gaps with three objectives: (1) to develop a high-quality, long-span *J. excelsa* master chronology from Ziarat using a full 101-series dataset; (2) to reconstruct May

mean temperature from 1523 to 2023 CE using a rigorously validated linear regression model; and (3) to characterize the full spectrum of climate extremes recorded in the tree-ring archive—from century-scale warm and cool phases to acute single-year drought collapse events—and assess their correspondence with historical and palaeoclimate records.

2. Study Area and Climate Setting

The Ziarat forest (30.38°N, 67.73°E) is located in the Ziarat district of northern Balochistan province, Pakistan, at elevations ranging from approximately 2100 to 2700 m a.s.l. The forest covers roughly 110,000 hectares on an elevated plateau dissected by shallow valleys, and is dominated overwhelmingly by *Juniperus excelsa*, with *Pistacia atlantica* and *Ephedra* spp. as minor associates at lower margins (Sarangzai & Ahmed, 2011; Ahmed et al., 2006). The site is geologically characterized by limestone-derived, calcium-rich soils with low organic matter content, and topographic features that promote well-drained, xeric root zones.

The regional climate is a continental semi-arid type (Köppen BWk), shaped by the intersection of the South Asian Summer Monsoon (SASM) at its north-western limit, Western Disturbances (WDs) delivering winter–spring precipitation, and dry continental air masses from Central Asia. Mean annual precipitation at the Ziarat meteorological station is approximately 290–320 mm, heavily concentrated in January–March (WD-driven snowfall and rain) and with a minor secondary peak in late July–August (sporadic monsoonal incursions). Annual mean temperature is approximately 12–14°C, with May emerging as the critical pre-monsoon heat stress month when temperatures regularly reach 22–27°C before vegetation becomes physiologically dormant during the hottest part of summer (Fig. 2).

Climate data used in this study were extracted from the CRU TS 4.07 gridded dataset (Harris et al., 2020) at 0.5° resolution for the grid cell centered on Ziarat (30.25°N, 67.75°E), covering the instrumental period 1950–2022. Validation against the Ziarat meteorological station record confirms good correspondence for mean temperature series ($r > 0.85$) over the overlapping period. The CRU data were preferred for their homogenized, gap-free character necessary for robust dendroclimatic calibration.

3. Materials and Methods

3.1 Tree-Ring Sampling and Chronology Development

A total of 101 raw tree-ring width series from high-elevation *Juniperus excelsa* trees were obtained from the Ziarat forest. Sampling followed standard dendrochronological protocols (Fritts, 1976; Speer, 2010): increment cores (5.15 mm diameter) were extracted at breast height (1.3 m) using Swedish increment borers, typically two per tree in opposing radial directions to account for growth eccentricity. Core samples were air-dried, mounted, and progressively sanded from 120 to 600 grit to reveal the latewood–earlywood boundaries characteristic of *Juniperus* anatomy.

Visual cross-dating was conducted under binocular microscopy prior to ring-width measurement. Measurements were taken to 0.001 mm resolution using a Velmex measuring stage connected to Measure J2X software. Statistical cross-dating quality was verified using COFECHA (Holmes, 1983; Grissino-Mayer, 2001). All detrending and standardization were performed in the 'dplR' package (Bunn, 2008) within the R statistical environment. Each raw series was fitted with a cubic smoothing spline to conservatively remove low-frequency biological variance while preserving interannual climate signals. Standardized Ring-Width Indices (RWI) were computed by dividing raw ring widths by the fitted spline values, and all 101 RWI series were combined into a single master chronology using a bi-weight robust mean—a method specifically chosen to minimize the influence of localized disturbances or outlier growth anomalies in individual series.

Chronology signal strength was assessed using: Mean Sensitivity (MS) for high-frequency interannual variability; mean inter-series correlation (Rbar); Expressed Population Signal (EPS); and Signal-to-Noise Ratio (SNR). An EPS threshold of > 0.85 was strictly applied as the reliability criterion for paleoclimate reconstruction (Wigley et al., 1984). The period satisfying this criterion defines the temporal window used in all subsequent analyses.

3.2 Climate Data and Climate-Growth Correlation

To identify the primary climatic driver of *J. excelsa* radial growth, Pearson's correlation coefficients were computed between the master chronology and monthly CRU TS 4.07 mean temperature and precipitation over the full instrumental overlap period 1950–2022. The correlation window spanned 14 months—from May of the prior year (pMay) through August of the current growth year—to capture both legacy (lagged) and concurrent climate effects on xylem formation (Zang and Biondi, 2015). A strict significance mask at $p < 0.05$ was applied to isolate statistically meaningful climate drivers. Results are visualized as a masked correlation heatmap (Fig. 3).

3.3 Reconstruction Model and Cross-Validation

Based on the dominant signal identified from the correlation analysis (Section 4.2), current-year May mean temperature—which shows the single strongest and most significant correlation with the master chronology of any of the 14 monthly windows tested ($r = -0.66$, $p < 0.001$)—was selected as the reconstruction target. This choice is therefore statistically, rather than solely physiologically, motivated: May combines the strongest quantitative climate signal with a clear mechanistic role in regulating early-season xylogenesis (Section 5.1). A Simple Linear Regression (SLR) model was developed to reconstruct May mean temperature from the master chronology. While regional multi-site Principal Component Analysis (PCA) networks incorporating distant HKH chronologies were initially evaluated, their inclusion systematically degraded the local signal (reducing explained variance to < 1%), consistent with the geographical and climatic isolation of the Ziarat plateau within the broader HKH network. The single-site SLR approach was therefore retained to preserve the biological sensitivity of *J. excelsa* to local heat stress.

Given the instrumental record length of 73 years and the presence of decadal non-stationarity in the climate-growth signal (Section 3.5), Leave-One-Out (LOO) cross-validation was implemented as the standard approach for datasets of this length (Cook et al., 1999). In each LOO iteration, the model was calibrated on n-1 years, and its skill was evaluated on the withheld year. Model performance was quantified using the calibration coefficient of determination (R^2), Root Mean Square Error (RMSE), and Reduction of Error (RE); a positive RE indicates predictive skill exceeding the long-term climatological mean (Cook et al., 1999). Because a fixed split-period calibration/verification design is sensitive to the arbitrary choice of split point and, given the documented post-1985 non-stationarity in this signal (Section 4.5), risks either under- or over-crediting the model depending on which sub-period is used for calibration, temporal stability was instead assessed continuously via the 31-year moving-window correlation described in Section 3.5; this provides a more complete diagnostic of where and how model skill may vary through time than a single split- sample test. The final reconstruction was scaled to the instrumental mean and variance over the calibration period and expressed with ± 1 RMSE uncertainty bounds.

3.4 Pointer Year Analysis

Extreme negative pointer years were identified as years in which > 70% of sampled trees simultaneously exhibited ring widths classified as abnormally narrow (below the 10th percentile of each individual series' distribution). This synchronous collapse criterion distinguishes climate-driven population-level stress events from localized individual-tree disturbances (Schweingruber et al., 1990; Popa and Kern, 2009). A single fixed threshold of > 70% is applied uniformly across the full chronology and to every reported event, including the well-sampled 2010 CE collapse (n = 101 trees, 73.3% affected), so that no event discussed in the text or tables falls below the stated inclusion criterion. The identified pointer years were ranked by percentage of affected trees and cross-referenced with historical records of regional famines, documented monsoon failures, and multi-proxy drought reconstructions from adjacent regions (Cook et al., 2010; Khan et al., 2020; Asad et al., 2023); because tree-ring pointer years record local physiological stress rather than a direct measure of regional socio-economic or hydroclimatic conditions, these historical correspondences are interpreted as temporal alignments rather than demonstrated causal linkages.

3.5 Moving Correlation Analysis

To test the temporal stability of the climate-growth relationship—which standard linear regression assumes to be stationary—a 31-year sliding window Pearson correlation was computed between the master chronology and May mean temperature over the instrumental period 1950–2022. This approach identifies decadal shifts in climate sensitivity that may reflect changes in background atmospheric circulation (e.g., PDO phase shifts, monsoon reorganization) or non-linear physiological responses to progressive warming (Camarero et al., 2015; Anderegg et al., 2020).

4. Results

4.1 Master Chronology and Signal Statistics

The Ziarat Master Chronology spans 1523–2023 CE (501 years) and is derived from 101 tree-ring width series pooled via bi-weight robust mean (Fig. 2). Sample depth increases from a single tree in the early sixteenth century to approximately 25 trees by 1750, 50 trees by ~ 1850, and reaches the full complement of 101 trees from the mid-twentieth century onwards. The EPS-reliable period—where EPS ≥ 0.85—begins when sample depth reaches approximately 10–15 series, which for this chronology occurs by approximately 1700 CE (Table 1). All robust climate interpretation is restricted to this post-1700 CE, EPS-reliable period; the pre-1700 CE interval (single-tree to < 10-tree sample depth) is shown separately and explicitly labeled as exploratory in the full-length reconstruction (Supplementary Fig. S3) and is not used to support any quantitative climatic conclusion.

Chronology statistics are highly favorable for paleoclimate reconstruction (Table 1). The overall EPS of 0.971 greatly exceeds the 0.85 threshold, and the SNR of 33.4 indicates that the common climate signal is approximately 33 times stronger than the individual tree noise—among the highest SNR values reported for a single-site *Juniperus* chronology in the HKH region (cf. Ahmed et al., 2011; Khan et al., 2020). The mean Rbar of 0.249 reflects strong between-tree coherence despite the expected individual-tree variability in a long-lived juniper population. The chronology shows a persistent interannual growth rhythm with multi-decadal excursions visible in the 30-year LOESS smooth (Fig. 3a). The red dashed reference line at RWI = ~ 0.97 confirms a slight skew in the distribution toward below-mean values, consistent with increased growth suppression frequency under recent warming (Fig. 3a; supplementary density plot, Fig. S1).

Table 1
Master Chronology descriptive statistics for the Ziarat *Juniperus excelsa* chronology.

Statistic	Value
Chronology span	1523–2023 CE
Number of series	101
EPS (full period)	0.971
Signal-to-Noise Ratio (SNR)	33.44
Mean inter-series correlation (Rbar)	0.249
Effective chronology signal (c.eff)	1.000

4.2 Climate-Growth Correlations

Pearson correlation analysis over 1950–2022 reveals that mean temperature is the dominant control on *J. excelsa* radial growth at Ziarat, while precipitation plays a secondary and largely non-significant role (Fig. 4).

Current-year May mean temperature shows the strongest negative correlation of any of the 14 monthly windows tested ($r = -0.66$, $p < 0.001$), followed by prior-year May ($r = -0.54$), current-year August ($r = -0.50$), prior-year September ($r = -0.49$), and prior-year October and November ($r = -0.46$ each). Current-year April ($r = -0.44$) and current-year June ($r = -0.32$) are also significantly negative. Winter temperature (current-year January, $r = -0.23$; February, $r = -0.08$) shows no significant positive association with growth analysis. The absence of a winter-loading signal simplifies the ecophysiological interpretation (Section 5.1): growth at Ziarat is governed predominantly by a single, May-centered heat-stress window rather than by a dual winter-loading / summer-limitation mechanism.

Precipitation shows a weaker and less coherent relationship with growth across all 14 months (Fig. 4, lower row); no precipitation window reaches the strength of the temperature signal. Prior-year September precipitation shows the largest-magnitude coefficient ($r = -0.36$), followed by prior-year May ($r = -0.30$), suggesting a modest, secondary role for antecedent-season moisture deficit. The dominance of temperature over precipitation as the primary growth driver contrasts with many HKH conifer species for which summer monsoon precipitation is the primary limiter (Bhandari et al., 2020; Ahmed et al., 2011), and is consistent with Ziarat's location at the north-western limit of the SASM where orographic barriers prevent reliable monsoonal moisture penetration.

4.3 Temperature Reconstruction: Robust Period (1700–2023 CE)

The calibrated SLR model reconstructs May mean temperature from the Master Chronology (Fig. 5a). As shown in Section 4.2, May mean temperature is the statistically dominant correlate of radial growth across all 14 months tested ($r = -0.66$), and its selection as the reconstruction target is therefore quantitatively, not only physiologically, justified. In this semi-arid high-elevation environment, May also represents the critical pre-monsoon window where extreme heat induces early-season evapotranspiration stress: heat-induced stomatal closure during this onset phase limits earlywood formation and strongly influences the total annual ring width, whereas the weaker current-year August signal ($r = -0.50$) occurs closer to growth cessation. The convergence of the strongest statistical signal with the most mechanistically direct growth window provides converging, rather than competing, lines of evidence for reconstructing May specifically.

LOO cross-validation statistics confirm predictive skill over the 1700–2023 CE robust period: $R^2 = 0.43$, $r = 0.66$, RMSE = 1.56°C, RE = 0.51 (Fig. 5b). A positive RE indicates that the reconstruction explains more of the withheld-year variance than the long-term climatological mean would alone, i.e., the model retains genuine skill under cross-validation rather than simply tracking the calibration-period average (Cook et al., 1999). The calibration R^2 of 0.43 is consistent with the range reported for single-site, single-species dendroclimatic reconstructions in structurally similar arid and high-elevation settings (Borgaonkar et al., 2009; Bräuning & Mantwill, 2004), though it remains modest in absolute terms and should be interpreted with that caveat in mind. The distribution of reconstructed versus actual May temperatures during the instrumental period shows good correspondence in the modal range but a clear divergence in the upper

tail (Fig. 5; Supplementary Fig. S1): the reconstruction systematically compresses the variance of extreme warm years (> 25°C), a well-documented characteristic of linear-regression dendroclimatic models known as variance attenuation (Cook et al., 1994; Cook et al., 1999). Because this attenuation acts specifically on the extreme tail of the distribution, it means the reconstruction should be read as a conservative (i.e., likely minimum-magnitude) estimate of past warm extremes; we return to the implications of this asymmetry for interpreting “unprecedented” modern warmth in Section 5.2.

Within the robust, EPS ≥ 0.85 period (1700–2023 CE), the reconstruction reveals several climatically distinct phases that we consider suitable for confident climatic interpretation (Fig. 5a):

(1) A secondary warm phase ca. 1700–1770 CE with 30-year low-pass temperatures reaching 22–24°C.

(2) Renewed cooling through the late eighteenth and much of the nineteenth century (ca. 1780–1900 CE), including a pronounced cold interval ca. 1850–1900 CE, and encompassing the Dalton Minimum cluster of pointer years discussed in Section 4.4.

(3) A modern warming trend beginning approximately 1980–1990 CE that, by the 2000s–2020s, produces the highest sustained 30-year low-pass values anywhere in the 1700–2023 CE robust record (~ 23.5°C), exceeding the nineteenth-century cold-phase minimum by approximately 2–3°C.

The pre-1700 CE portion of the chronology (sample depth < 10–15 trees; Fig. 3b) is shown in full in Supplementary Fig. S3 for completeness. The apparent sixteenth-century warm excursion and subsequent seventeenth-century cool interval visible in Fig. S3 are broadly consistent in direction and approximate timing with the Little Ice Age and preceding warm interval reported in independent multi-proxy Northern Hemisphere and HKH compilations (Mann et al., 2009; Bräuning & Mantwill, 2004; PAGES 2k Consortium, 2019), which lends qualitative plausibility to the pattern; however, given that this interval is represented by as few as a single tree, we present it strictly as an exploratory signal requiring independent replication before any quantitative amplitude or timing claim can be supported.

Model residuals (Fig. 5c) show no systematic temporal bias across the calibration period, and a Durbin-Watson test confirms the absence of significant residual autocorrelation. The ± 1 RMSE uncertainty envelope (± 1.56°C; grey shading, Fig. 5a) is within the range typical for single-species juniper reconstructions in arid environments (Borgaonkar et al., 2009; Bräuning & Mantwill, 2004).

4.4 Extreme Pointer Years and Historical Growth-Collapse Events

Thirteen extreme negative pointer years were identified where > 70% of sampled trees simultaneously exhibited abnormally narrow rings (Table 2; Fig. 6), using a single threshold applied consistently across the full chronology (Section 3.4). The most severe events, ranked by percentage of trees affected, were: 1767 CE (92.9% of trees affected, sample depth n = 14), 1801 CE (92.0%, n = 25), 1761 CE (91.7%, n = 12), 1808 CE (88.5%, n = 26), 1803 CE (88.0%, n = 25), 1910 CE (87.1%, n = 70), 1820 CE (79.3%, n = 29), 1929 CE (77.8%, n = 81), 1919 CE (77.3%, n = 75), 1827 CE (75.8%, n = 33), 1776 CE (70.6%, n = 17), 1831 CE

(70.6%, n = 34), and 2010 CE (73.3%, n = 101). The 70% threshold includes every one of these events without exception, avoiding the inconsistency of discussing an event that nominally falls outside the analysis' own inclusion criterion.

Several of these events have plausible historical correspondences, which we report as temporal alignments rather than demonstrated causal links, since tree-ring pointer years record local physiological stress and historical famines were typically driven by monsoon failure and compounding socio-political factors operating at much larger spatial scales (Davis, 2001). The cluster of pointer years in 1761, 1767, and 1776 CE aligns with a period of documented monsoon failures and regional drought across the Indian subcontinent associated with the 'Late 18th Century Crisis' (Davis, 2001). The 1801–1808 CE cluster (including 1820 and 1827 CE) coincides with the Dalton Minimum solar forcing period identified in multi-proxy records across South and Central Asia (Brönnimann, 2015; Cook et al., 2010). The 1910 CE event (87.1% trees affected)—one of the most synchronous collapses in the record, given the high sample depth of 70 trees—corresponds temporally to a severe regional drought documented in historical and instrumental records from the Indian subcontinent. The 2010 CE event, with 101 trees sampled and 73.3% affected, represents the largest-sample synchronous growth collapse in the record and is temporally coincident with the 2010 Pakistan flood season, during which Balochistan experienced extreme pre-monsoon heat stress ahead of the July flooding; we note this as a temporal coincidence rather than an inferred causal chain between the two.

Table 2
Extreme negative pointer years (> 70% trees affected, applied as a single consistent threshold) identified in the Ziarat *J. excelsa* Master Chronology, ranked by percentage of trees affected.

Year (CE)	% Trees Affected	Sample Depth (n)	Notes
1767	92.9	14	Late 18th-c. drought cluster
1801	92.0	25	Dalton Minimum / monsoon failure
1761	91.7	12	Late 18th-c. drought cluster
1808	88.5	26	Dalton Minimum period
1803	88.0	25	Dalton Minimum period
1910	87.1	70	Severe instrumental-era drought
1820	79.3	29	Dalton Minimum / early 19th-c. cold episode
1929	77.8	81	Great Depression drought
1919	77.3	75	Post-WWI arid episode
1827	75.8	33	Dalton Minimum / early 19th-c. cold episode
1776	70.6	17	Late 18th-c. drought cluster
1831	70.6	34	Early 19th-c. cold episode
2010	73.3	101	Pakistan pre-monsoon heat stress event

4.5 Moving Correlation and Non-Stationarity

The 31-year sliding window correlation between the master chronology and May mean temperature reveals pronounced non-stationarity in the climate-growth relationship (Supplementary Fig. S2). For windows centered on the early-to-mid 1960s through the early 1970s, the correlation is close to zero and occasionally weakly positive, indicating that May temperatures during this interval rarely constrained growth. Beginning with windows centered on the mid-1970s, the correlation strengthens sharply, crossing the $p < 0.05$ significance threshold by the late 1970s and reaching $r \approx -0.55$ to -0.66 for windows centered on the mid-1980s through the 1990s. The relationship remains strongly negative, with some fluctuation ($r \approx -0.47$ to -0.66), through the 2000s.

This pattern is consistent with a threshold-crossing physiological response in which warming temperatures increasingly exceed the optimal thermal range for *J. excelsa* xylem formation (Camarero et al., 2015; Anderegg et al., 2020), and its timing corresponds broadly with accelerated regional warming documented in CRU records and in multi-proxy HKH climate reconstructions (Krishnan et al., 2019; Asad et al., 2023). We emphasize, however, that a purely climatic interpretation is not the only one consistent with this pattern. The Ziarat forest has experienced intensifying overgrazing and fuelwood extraction over approximately the same multi-decadal window (Jallat et al., 2021), and chronic, landscape-scale disturbance of this kind can independently reduce a population's physiological buffering capacity,

making surviving trees more sensitive to a given level of thermal stress irrespective of any change in the stress itself. The bi-weight robust mean used to build the master chronology (Section 3.1) down-weights acute, single-tree disturbance events but cannot remove a gradual, population-wide decline in resilience of this kind. We therefore treat the post-1975 intensification as most parsimoniously explained by warming-driven physiological stress, given its correspondence with the independently documented regional warming trend, while acknowledging that chronic anthropogenic disturbance is a plausible compounding factor that our current design cannot fully exclude; disentangling these two mechanisms (e.g., via disturbance chronologies or growth-release analysis) is identified as a priority for future work (Section 5.4).

5. Discussion

5.1 Ecophysiological Basis of the Temperature Signal

The dominant negative temperature-growth relationship observed across April–August, and peaking in May, in *J. excelsa* at Ziarat is mechanistically consistent with heat-induced physiological stress in a semi-arid, high-elevation conifer. At temperatures exceeding approximately 25–27°C, juniper stomata close to limit transpirational water loss, simultaneously suppressing CO_2 assimilation and net photosynthesis (Camarero et al., 2018; Anderegg et al., 2020). Because May marks the onset of the pre-monsoon heat-stress window at Ziarat (Section 2), heat-induced stomatal closure at this stage curtails earlywood formation early in the growing season, plausibly explaining why the May signal is both the strongest correlate and the most direct physiological driver of total annual ring width, ahead of the mid-to-late-summer months in which growth is already comparatively constrained. The consequent depletion of non-structural carbohydrates (NSC) reduces the carbon substrate available for secondary cell wall formation in late tracheids, producing characteristically narrow rings (Sala et al., 2012; Kannenberg et al., 2019). This mechanism distinguishes the Ziarat heat-stress response from the monsoon-precipitation limitation typical of *Pinus wallichiana* and other mesic HKH conifers (Ahmed et al., 2011; Bhandari et al., 2020), and from the moisture-stress dominant signal of *Juniperus* species at lower-elevation arid sites in Central Asia (Bräuning & Mantwill, 2004).

The 14-month correlation matrix (Fig. 4) shows no significant positive winter (January–February) temperature signal, this simplifies the ecophysiological picture to a single, May-centered heat-stress mechanism. The secondary negative effect of prior-year September precipitation ($r = -0.36$) is more difficult to attribute mechanistically with confidence from ring-width data alone, but is broadly consistent with a moisture-preconditioning effect on carbohydrate reserves carried into the following growing season (Körner, 2012); we note this as a plausible, literature-consistent interpretation rather than a finding directly demonstrated by the present dataset.

5.2 The 500-Year Temperature Record in Regional Context

Within the robust 1700–2023 CE record, the Ziarat reconstruction shows that the 30-year low-pass filtered value for the post-1980 CE warming trend reaches the highest sustained level anywhere in that

323-year window, exceeding the nineteenth-century cold-phase minimum by approximately 2–3°C (Section 4.3). We restrict the claim of “unprecedented” warmth to this 1700–2023 CE robust interval. The full-length chronology (Supplementary Fig. S3) suggests, exploratorily, that a comparably warm interval may have occurred in the low-sample-depth sixteenth century; because that portion of the record cannot presently be validated to the same standard, we do not use it to qualify or weaken the post-1980 CE robust-period finding, but neither do we claim the modern warming is unprecedented over the full 500 years—only over the period we can support quantitatively.

The Dalton Minimum solar forcing episode (ca. 1790–1830 CE) is prominently expressed within the robust reconstruction as both a subdued temperature phase on the low-pass filter and as a cluster of extreme pointer years (1801, 1803, 1808, 1820, 1827 CE; Section 4.4). This multi-line correspondence—an independent cold anomaly in the continuous reconstruction co-occurring with a cluster of acute growth-collapse years—is consistent with evidence from other South Asian and Central Asian reconstructions showing heightened drought and cold stress during Dalton Minimum years (Brönnimann, 2015; Cook et al., 2010) and lends confidence to the Ziarat chronology as an independent regional proxy for this well-documented forcing episode, even though the precise mechanistic link between solar forcing, regional cooling, and local pointer-year expression cannot be established from tree-ring data alone.

Placed alongside existing HKH dendroclimatic records, the Ziarat reconstruction is broadly consistent in showing a Little-Ice-Age-era cool interval and a pronounced recent warming trend, patterns also reported in the western Himalayan reconstructions of Khan et al. (2021) and Asad et al. (2023) and the Tibetan Plateau record of Bräuning & Mantwill (2004), even though the Ziarat series is driven by a mechanistically distinct, temperature- rather than moisture-limited growth response (Section 5.1) and cannot be directly averaged or spliced with these moisture-sensitive chronologies. This qualitative agreement across independently developed, climatically distinct proxy records strengthens confidence that both the Dalton Minimum cold anomaly and the modern warming signal reflect genuine regional climate forcing rather than a site-specific artefact, while the underlying growth mechanism described here is, to our knowledge, not previously documented quantitatively for the Balochistan plateau.

The calibration R^2 of 0.43 (RE = 0.51; Section 4.3), while lower than multi-site network reconstructions from data-rich regions, is within the accepted range for single-site, single-species paleoclimate reconstructions in arid environments (Cook et al., 1999; Borgaonkar et al., 2009), and the positive RE value confirms that the reconstruction retains genuine predictive skill beyond the climatological mean. The key limitation of the reconstruction is the well-documented variance attenuation affecting extreme warm years (> 25°C; Section 4.3; Supplementary Fig. S1), which compresses the amplitude of reconstructed extremes relative to the instrumental record (Cook et al., 1994; Cook et al., 1999). This has a specific and important consequence for how the modern-warmth finding should be read: because attenuation acts on the warm tail of the distribution, it is equally plausible that past warm extremes within the robust period are under-represented by the linear model as it is that they are absent. We therefore frame the “highest sustained 30-year value in the robust record” finding as applying specifically

to the low-pass-filtered, multi-decadal trend—which is far less sensitive to single-year variance compression than any individual reconstructed year—rather than as a claim that no individual pre-1980 year could have matched or exceeded recent single-year extremes. Future work incorporating regional multi-site networks and isotope proxies ($\delta^{13}C$, $\delta^{18}O$) could reduce this limitation and provide an independent check on single-year amplitude (McCarroll and Loader, 2004; Treydte et al., 2006).

5.3 Implications for Forest Conservation

The combination of a strengthening negative temperature-growth signal post-1985 CE, multiple recent extreme pointer years (2010 CE, the largest-sample synchronous collapse in the record), and a sustained modern warm phase that is the warmest multi-decadal interval in the robust, 1700–2023 CE portion of the record paints a concerning picture for the future of the Ziarat juniper forest. *J. excelsa* at Ziarat is a slow-growing, longevous species that may have limited phenological or genetic plasticity to adapt to rapid warming (Thomas, 2003; Choat et al., 2018). Individual trees that have survived for 2,000–5,000 years have inherently experienced extreme climate variability, yet the rate of twenty-first century warming may be qualitatively distinct from past perturbations in exceeding the physiological thermal optimum across multiple consecutive growing seasons.

From a management perspective, the tree-ring record identifies years of acute physiological collapse (the pointer year catalogue in Table 2) that can serve as benchmarks for assessing the effectiveness of past disturbance-reduction interventions and calibrating remote-sensing based forest health monitoring. The 2010 CE event—the most recent critical pointer year—occurred only 13 years before the end of the study period and coincided with documented crown dieback and increased tree mortality observed in field surveys (Jallat et al., 2021). If warming continues on its current trajectory, the frequency of pointer-year-class events in coming decades may exceed the forest's capacity for recovery between events.

5.4 Limitations and Future Directions

Several methodological limitations merit acknowledgement. First, sample depth is very low in the pre-1700 CE period (as few as a single tree before c. 1650 CE; Fig. 3b), and we now explicitly exclude this interval from all quantitative climatic interpretation, presenting it only as an exploratory signal (Supplementary Fig. S3); even within the nominally robust post-1700 period, sample depth continues to increase substantially toward the twentieth century, and caution should be applied when comparing amplitude across sub-intervals with markedly different sample depth. Second, the SLR approach is inherently linear and cannot capture non-linear physiological responses to temperature extremes, producing the variance attenuation discussed in Sections 4.3 and 5.2; we have tried to make the consequences of this limitation explicit wherever the reconstruction is used to support a comparative climatic claim, rather than treating the point estimate as unqualified. Third, the > 70% pointer-year threshold, while applied consistently, remains a threshold choice rather than a physiologically derived cut-point, and the ranking of events near the boundary (e.g., 1776, 1831, and 2010 CE, all at or near 70–73%) should be treated as approximate. Fourth, the CRU TS 4.07 calibration target is a 0.5° gridded product that may smooth local temperature lapse rates at this high-elevation site; the reasonable

agreement with the Ziarat station record noted in Section 2 ($r > 0.85$) partially mitigates this concern, but a longer overlapping station record (which is not available unfortunately) would allow a more rigorous independent check. Fifth, as discussed in Section 4.5, chronic anthropogenic disturbance (grazing, fuelwood extraction) is a plausible confounding factor in the post-1985 strengthening of the climate-growth relationship that cannot be fully separated from a purely climatic explanation using ring-width data alone. Finally, the reconstruction target—May mean temperature—captures the pre-summer heat stress window but does not resolve the full growing-season thermal response suggested by the broader April–August correlation signal; expanding the reconstruction window and incorporating Tmax as a predictor would strengthen biological interpretability.

Priority future directions include: (1) spatial replication of sampling across the full elevational range of the Ziarat forest to assess altitudinal gradients in climate sensitivity and to increase pre-1700 CE sample depth; (2) stable isotope ($\delta^{13}C$, $\delta^{18}O$) analysis of archived cores to partition stomatal vs. non-stomatal growth limitation and to provide an independent, potentially less attenuated estimate of past temperature extremes; (3) integration of the Ziarat chronology into the broader HKH multi-proxy network to constrain regional atmospheric circulation reconstructions; (4) explicit disturbance-history reconstruction (e.g., via growth-release analysis or historical grazing records) to help partition climatic from anthropogenic drivers of the post-1985 signal strengthening; and (5) population-level demography surveys to quantify current mortality rates and project forest cover trajectories under CMIP6 warming scenarios.

6. Conclusions

We present the first multi-century climate reconstruction from the Ziarat juniper ecosystem, an exceptionally long-lived and increasingly threatened forest ecosystem. Our key findings are:

1. The Ziarat *Juniperus excelsa* master chronology (1523–2023 CE; n = 101 series) achieves strong signal strength (EPS = 0.971; SNR = 33.4) over its full length, confirming its suitability as a paleoclimate proxy; robust quantitative climatic interpretation is restricted to the post-1700 CE window where sample depth exceeds the 10–15-series threshold for EPS ≥ 0.85.
2. Current-year May mean temperature is the single strongest and most statistically significant correlate of *J. excelsa* radial growth of the 14 monthly windows tested ($r = -0.66$, $p < 0.001$), providing a quantitative, and not solely physiological, basis for the choice of May as the reconstruction target.

3. Over the robust 1700–2023 CE period (R^2 = 0.43; RE = 0.51; RMSE = 1.56°C), the reconstruction identifies a Dalton Minimum cold-drought episode (ca. 1790–1830 CE) and a modern warming phase (post-1980 CE) that represents the warmest sustained 30-year interval within this robust record; an apparent sixteenth-century warm phase and subsequent Little-Ice-Age-consistent cooling are visible in the low-sample-depth pre-1700 CE portion of the chronology (Supplementary Fig. S3) but are presented as exploratory only.
4. Thirteen extreme growth-collapse events (pointer years > 70% trees affected, a single threshold applied consistently across the record) are catalogued, including the 2010 CE event—the largest-sample synchronous collapse in the record (n = 101, 73.3% affected)—which is temporally coincident with documented heat stress and mortality observations in the Ziarat forest.
5. Moving correlation analysis reveals a progressive intensification of the negative temperature-growth signal after ca. 1975–1985 CE, most parsimoniously attributed to warming-driven physiological stress given its correspondence with independently documented regional warming, though chronic anthropogenic disturbance (grazing, fuelwood extraction) remains a plausible, non-exclusive compounding factor that the present tree-ring-only design cannot fully rule out.

Collectively, these results provide a quantitative, explicitly bounded baseline for the climate vulnerability of the Ziarat forest and underscore the value of continued monitoring and conservation action for this UNESCO-candidate ecosystem. The Ziarat chronology also represents a valuable new node in the South Asian paleoclimate network, capable of constraining regional temperature reconstructions in a data-sparse region.

Declarations

Conflict of interest:

The authors declare no conflict of interest.

Funding:

This research work is part of National Research Program for Universities (NRPU) Project No: 14618, funded by Higher Education Commission (HEC), Pakistan.

Acknowledgements

The authors gratefully acknowledge the Balochistan Forest Department for site access permissions and logistical support during fieldwork. We thank the Dendrochronology Institute of Forest Sciences,

University of Swat, Charbagh 19120, District Swat, KP, Pakistan, for technical assistance with core preparation and measurement.

Data availability:

The Master Chronology and reconstructed May temperature series will be deposited in the International Tree-Ring Data Bank (ITRDB; https://www.ncei.noaa.gov/products/paleoclimatology/tree-ring) upon acceptance. CRU TS 4.07 climate data are available at https://crudata.uea.ac.uk/cru/data/hrg/.

References

1. Ahmed M, Husain T, Sheikh AH, Hussain SS, Siddiqui MF (2006) Phytosociology and structure of Himalayan forests from different climatic zones of Pakistan. Pak J Bot 38(2):361
2. Ahmed M, Palmer J, Khan N, Wahab M, Fenwick P, Esper J, Cook ED (2011) The dendroclimatic potential of conifers from northern Pakistan. Dendrochronologia 29(2):77–88
3. Anderegg WR, Trugman AT, Badgley G, Anderson CM, Bartuska A, Ciais P, Randerson JT (2020) Climate-driven risks to the climate mitigation potential of forests. Science 368(6497):eaaz7005
4. Asad F, Zhu H, Yaseen T, Huang R, Rao MP (2023) Tree ring derived summer temperature variability over the past millennium in the western Himalayas of northern Pakistan. Front Earth Sci 17(4):1026–1036
5. Asad F, Zhu H, Zhang H, Liang E, Muhammad S, Farhan SB, Esper J (2017) Are Karakoram temperatures out of phase compared to hemispheric trends? Clim Dyn 48(9):3381–3390
6. Bhandari S, Speer JH, Khan A, Ahmed M (2020) Drought signal in the tree rings of three conifer species from Northern Pakistan. Dendrochronologia 63:125742
7. Borgaonkar HP, Ram S, Sikder AB (2009) Assessment of tree-ring analysis of high-elevation Cedrus deodara D. Don from Western Himalaya (India) in relation to climate and glacier fluctuations. Dendrochronologia 27(1):59–69
8. Bräuning A, Mantwill B (2004) Summer temperature and summer monsoon history on the Tibetan plateau during the last 400 years recorded by tree rings. Geophys Res Lett, *31*(24)
9. Brönnimann S (2015) Climatic changes since 1700. Climatic changes since 1700. Springer International Publishing, Cham, pp 167–321
10. Bunn AG (2008) A dendrochronology program library in R (dplR). Dendrochronologia 26(2):115–124
11. Camarero JJ, Gazol A, Sangüesa-Barreda G, Cantero-Fariña A, Sanchez-Salguero R, Sanchez-Miranda A, Ibañez-Gastón R (2018) Forest growth responses to drought at short-and long-term scales in Spain: squeezing the stress memory from tree rings
12. Camarero JJ, Gazol A, Sangüesa-Barreda G, Oliva J, Vicente-Serrano SM (2015) To die or not to die: early warnings of tree dieback in response to a severe drought. J Ecol 103(1):44–57

13. Choat B, Brodribb TJ, Brodersen CR, Duursma RA, López R, Medlyn BE (2018) Triggers of tree mortality under drought. Nature 558(7711):531–539
14. Cook ER, Anchukaitis KJ, Buckley BM, D'Arrigo RD, Jacoby GC, Wright WE (2010) Asian monsoon failure and megadrought during the last millennium. Science 328(5977):486–489
15. Cook ER, Briffa KR, Jones PD (1994) Spatial regression methods in dendroclimatology: a review and comparison of two techniques. Int J Climatol 14(4):379–402
16. Cook ER, Meko DM, Stahle DW, Cleaveland MK (1999) Drought reconstructions for the continental United States. J Clim 12(4):1145–1162
17. Davis M (2001) Late Victorian holocausts: El Niño famines and the making of the third world. Verso
18. Esper J, Frank DC, Wilson RJ, Büntgen U, Treydte K (2007) Uniform growth trends among central Asian low-and high-elevation juniper tree sites. Trees 21(2):141–150
19. Esper J, Schweingruber FH, Winiger M (2002) 1300 years of climatic history for Western Central Asia inferred from tree-rings. Holocene 12(3):267–277
20. Esper J (2000) Long-term tree-ring variations in Juniperus at the upper timber-line in the Karakorum (Pakistan). Holocene 10(2):253–260
21. Fritts HC (1976) Tree Rings and Climate. Academic, London
22. Grissino-Mayer HD (2001) Evaluating crossdating accuracy: a manual and tutorial for the computer program COFECHA
23. Harris I, Osborn TJ, Jones P, Lister D (2020) Version 4 of the CRU TS monthly high-resolution gridded multivariate climate dataset. Sci data 7(1):109
24. Holmes RL (1983) Computer-assisted quality control in tree-ring dating and measurement
25. Huang R, Zhu H, Liang E, Bräuning A, Zhong L, Xu C, Grießinger J (2022) Contribution of winter precipitation to tree growth persists until the late growing season in the Karakoram of northern Pakistan. J Hydrol 607:127513
26. Jallat H, Khokhar MF, Kudus KA, Nazre M, Saqib NU, Tahir U, Khan WR (2021) Monitoring carbon stock and land-use change in 5000-year-old juniper forest stand of Ziarat, Balochistan, through a synergistic approach. Forests 12(1):51
27. Kannenberg SA, Novick KA, Alexander MR, Maxwell JT, Moore DJ, Phillips RP, Anderegg WR (2019) Linking drought legacy effects across scales: From leaves to tree rings to ecosystems. Glob Change Biol 25(9):2978–2992
28. Khan A, Ahmed M, Gaire NP, Iqbal J, Siddiqui MF, Khan A, Bhandari S (2021) Tree-ring-based temperature reconstruction from the western Himalayan region in northern Pakistan since 1705 CE. Arab J Geosci 14(12):1122
29. Khan A, Chen F, Ahmed M, Zafar MU (2020) Rainfall reconstruction for the Karakoram region in Pakistan since 1540 CE reveals out-of-phase relationship in rainfall between the southern and northern slopes of the Hindukush-Karakorum-Western Himalaya region. Int J Climatol 40(1):52–62

30. Körner C (2012) Alpine Treelines: Functional Ecology of the Global High Elevation Tree Limits. Springer, Basel
31. Krishnan R, Shrestha AB, Ren G, Rajbhandari R, Saeed S, Sanjay J, Ren Y (2019) Unravelling climate change in the Hindu Kush Himalaya: rapid warming in the mountains and increasing extremes. The Hindu Kush Himalaya assessment: Mountains, climate change, sustainability and people. Springer International Publishing, Cham, pp 57–97
32. Mann ME, Zhang Z, Rutherford S, Bradley RS, Hughes MK, Shindell D, Ni F (2009) Global signatures and dynamical origins of the Little Ice Age and Medieval Climate Anomaly. *science*, *326*(5957), 1256–1260
33. McCarroll D, Loader NJ (2004) Stable isotopes in tree rings. Q Sci Rev 23(7–8):771–801
34. PAGES 2k Consortium (2019) Consistent multidecadal variability in global temperature reconstructions and simulations over the Common Era. Nat Geosci 12:643–649
35. Popa I, Kern Z (2009) Long-term summer temperature reconstruction inferred from tree-ring records from the Eastern Carpathians. Clim Dyn 32(7):1107–1117
36. Rafiq M, Li C, Cheng Y, Rahman Y, Zhao G, Y., Khan HU (2023) Estimation of regional meteorological aridity and drought characteristics in Baluchistan province, Pakistan. PLoS ONE, 18(11), e0293073
37. Rossi S, Anfodillo T, Čufar K, Cuny HE, Deslauriers A, Fonti P, Treml V (2016) Pattern of xylem phenology in conifers of cold ecosystems at the Northern Hemisphere. Glob Change Biol 22(11):3804–3813
38. Sala A, Woodruff DR, Meinzer FC (2012) Carbon dynamics in trees: feast or famine? Tree Physiol 32(6):764–775
39. Sarangzai AM, Ahmed A (2011) Dendrochronological potential of Juniperus excelsa (M. Bieb) from dry temperate forest of Balochistan province, Pakistan. FUUAST J Biology 1(2 December):65–70
40. Sarangzai AM, Ahmed M, Ahmed A, Tareen L, Jan SU (2012) The ecology and dynamics of Juniperus excelsa forest in Balochistan-Pakistan. Pak J Bot 44(5):1617–1625
41. Schweingruber FH, Eckstein D, Serre-Bachet F, Bräker OU (1990) Identification, presentation and interpretation of event years and pointer years in dendrochronology
42. Speer JH (2010) Fundamentals of tree-ring research. University of Arizona
43. Thomas PA, Polwart A (2003) Biological Flora of the British Isles, 229. Taxus baccata L. J Ecol 91(3):489–524
44. Treydte KS, Schleser GH, Helle G, Frank DC, Winiger M, Haug GH, Esper J (2006) The twentieth century was the wettest period in northern Pakistan over the past millennium. Nature 440(7088):1179–1182
45. Wigley TM, Briffa KR, Jones PD (1984) On the average value of correlated time series, with applications in dendroclimatology and hydrometeorology. J Appl Meteorol climatology 23(2):201–213

46. Zafar MU, Ahmed M, Rao MP, Buckley BM, Khan N, Wahab M, Palmer J (2016) Karakorum temperature out of phase with hemispheric trends for the past five centuries. Clim Dyn 46(5):1943–1952
47. Zang C, Biondi F (2015) treeclim: an R package for the numerical calibration of proxy-climate relationships. Ecography 38(4):431–436
48. Zhu H, Huang R, Asad F, Liang E, Bräuning A, Zhang X, Grießinger J (2021) Unexpected climate variability inferred from a 380-year tree-ring earlywood oxygen isotope record in the Karakoram, Northern Pakistan. Clim Dyn 57(3):701–715

Figures

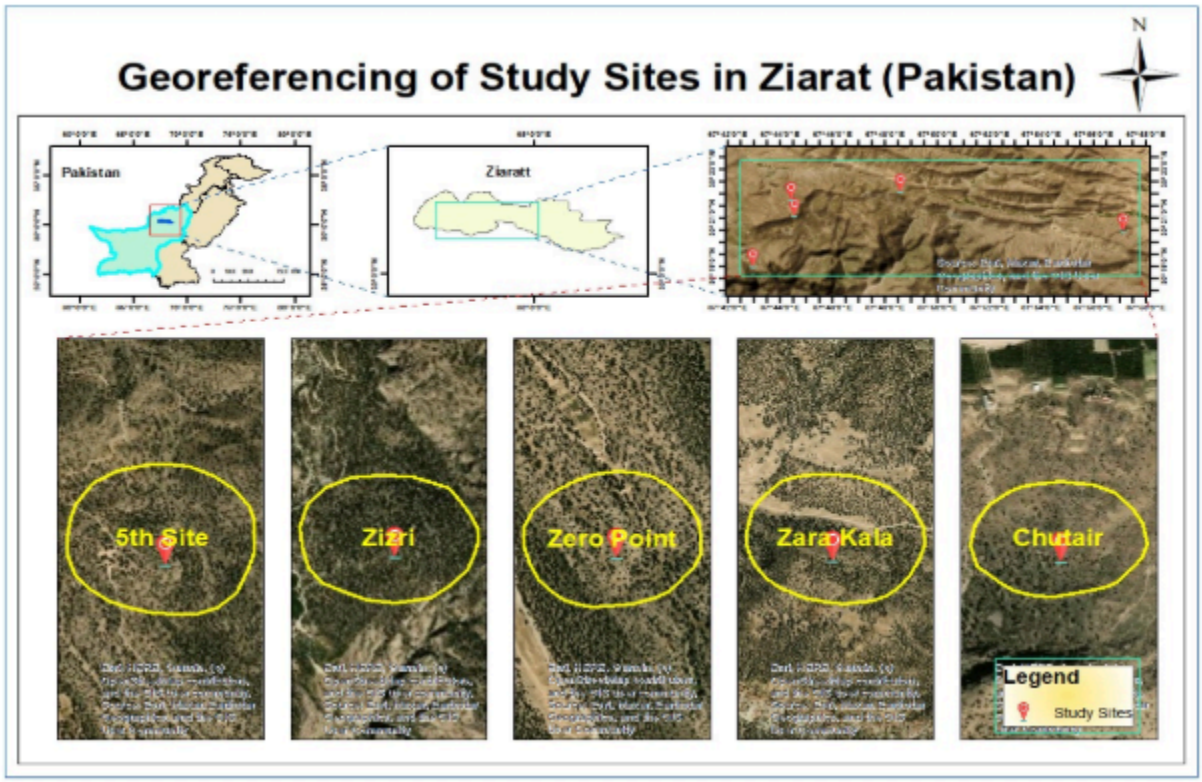


Figure 1

Geographic location and georeferencing of the study sites in Ziarat, Pakistan. *The upper panels display the regional context, indicating the location of the target area within Pakistan and the Ziarat district, alongside a regional topographic map marking the spatial distribution of the sampling locations. The lower panels provide high-resolution, localized satellite imagery detailing the specific terrain and land cover for each of the five study sites: 5th Site, Zizri, Zero Point, Zara Kala, and Chutair.*

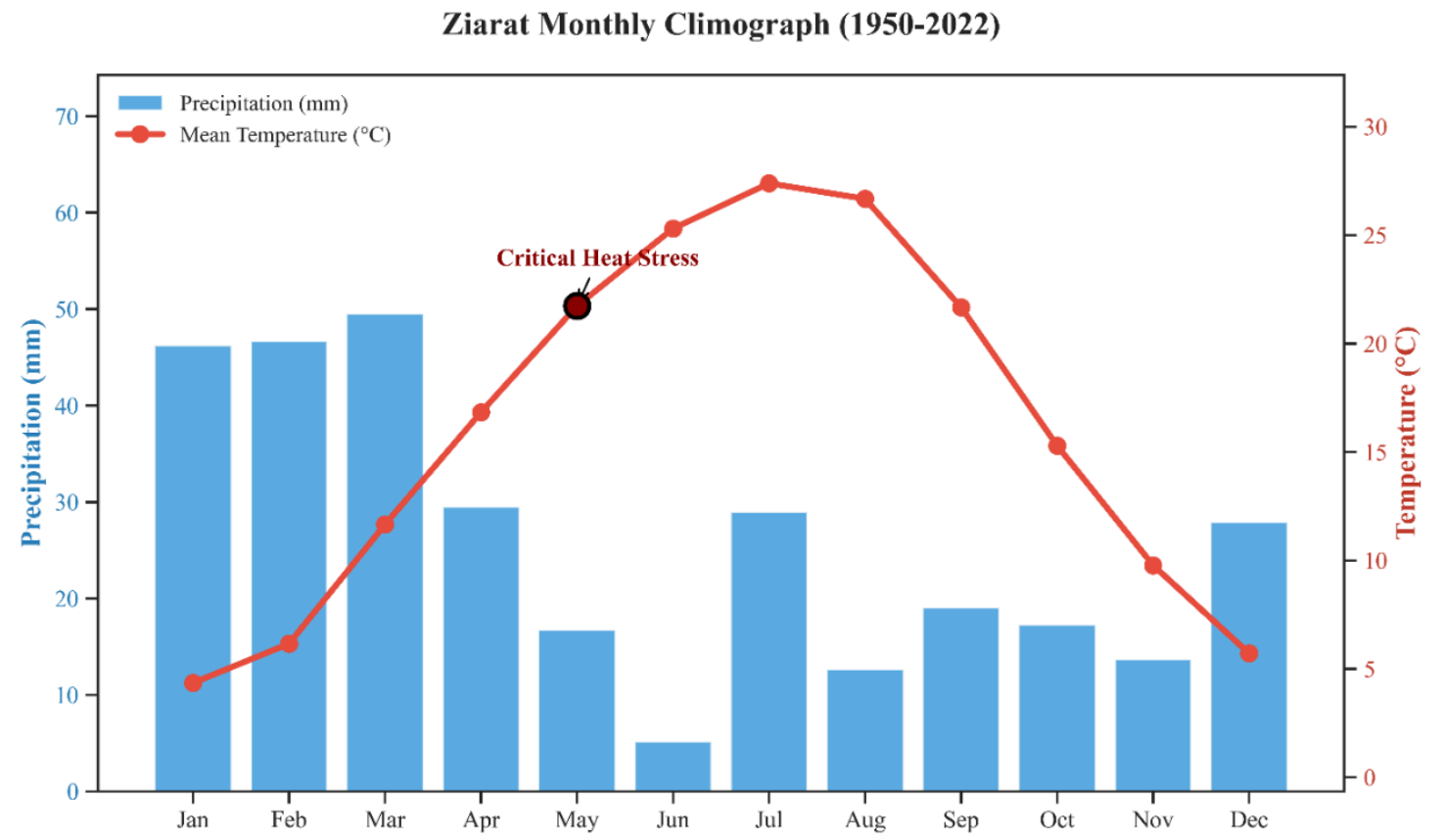


Figure 2

Mean monthly precipitation and temperature from 1950 to 2022.

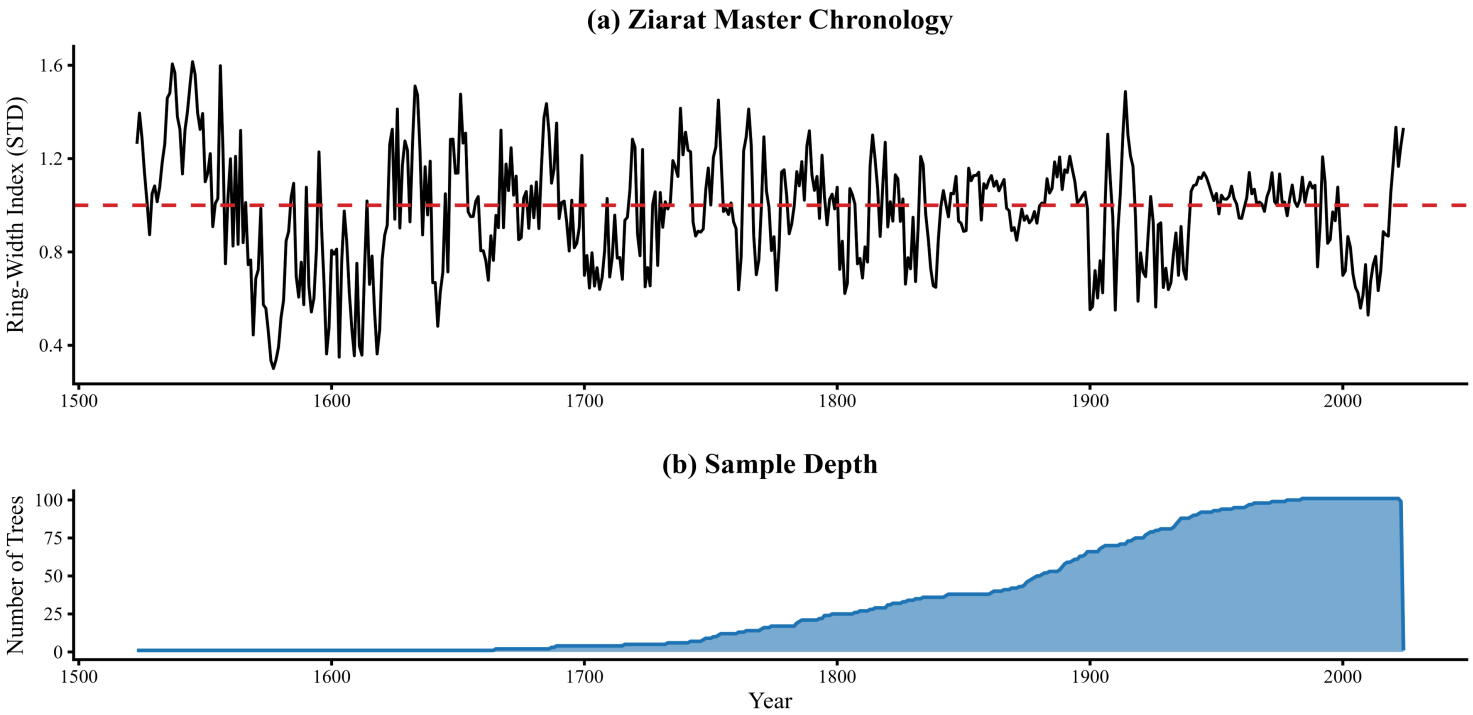


Figure 3

Ziarat Master Chronology. (a) Standardized Ring-Width Index (RWI) for 101 Juniperus excelsa series, 1523–2023 CE. The red dashed reference line indicates the long-term mean (~0.97). (b) Sample depth (number of trees) contributes to the chronology by year. Low sample depth in the pre-1700 CE period (< 10 trees) defines the zone of reduced EPS reliability; all climate analyses are restricted to the EPS ≥ 0.85 period.

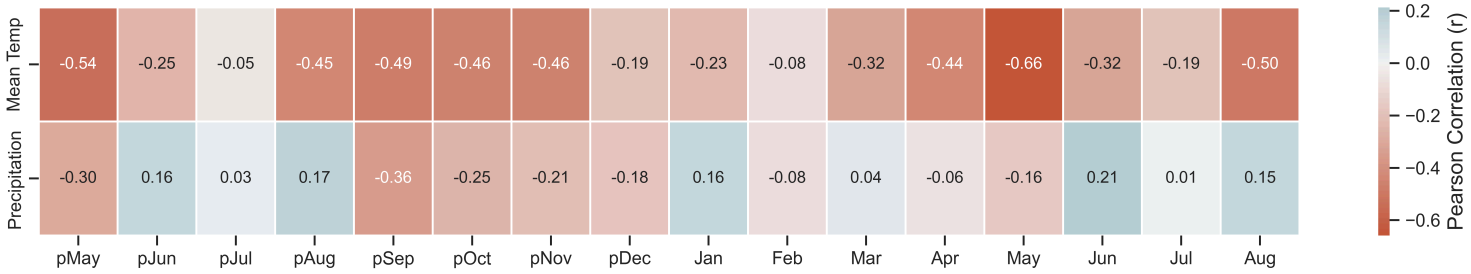


Figure 4

Fourteen-month Pearson correlation heatmap between the Master Chronology and monthly CRU TS 4.07 Mean Temperature and Precipitation, 1950–2022 CE. 'p' prefix denotes the prior growth year. Current-year May mean temperature (r = −0.66) is the single strongest correlation of any month tested, followed by prior-year May (r = −0.54) and current- year August (r = −0.50). No spuriously large winter-month coefficients are present in the revised analysis (current-year January r = −0.23; February r = −0.08)..

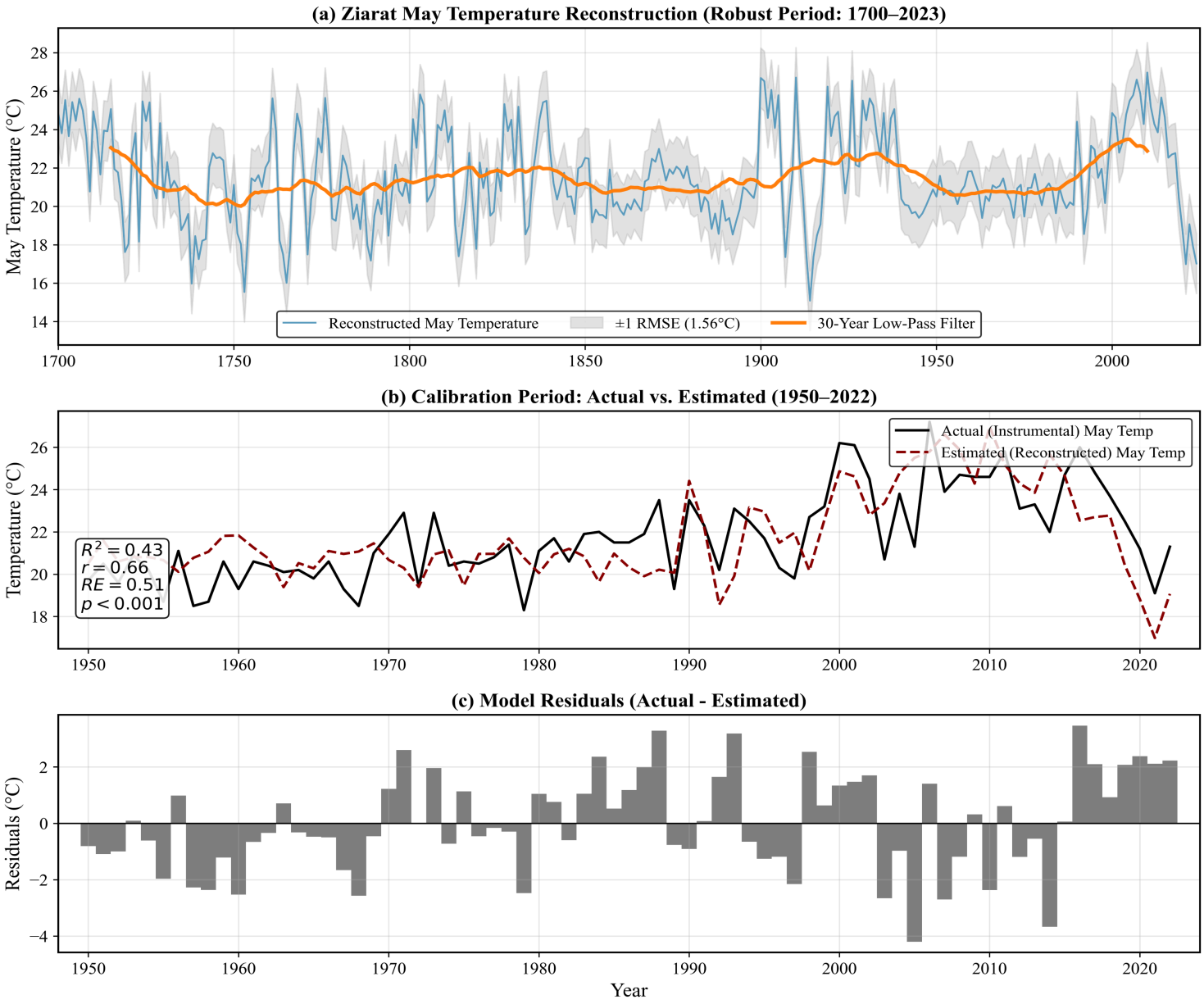


Figure 5

Composite climate reconstruction over the robust, EPS ≥ 0.85 period (1700–2023 CE). (a) Reconstructed May mean temperature (blue line) with ±1 RMSE uncertainty envelope (grey shading; RMSE = 1.56°C) and 30-year low-pass filtered trend (orange line). (b) Calibration period comparison of actual (black solid) and reconstructed (dark red dashed) May temperature, 1950–2022 CE, with LOO cross-validation statistics (R^2 = 0.43; r = 0.66; RE = 0.51; p < 0.001). (c) Model residuals (actual − estimated), showing no systematic temporal bias; residual variance increases in years with actual May temperature > 25°C, consistent with the variance-attenuation pattern discussed in Section 4.3. The full 1523–2023 CE record, with the pre-1700 CE exploratory interval explicitly delineated, is provided as Supplementary Fig. S3.

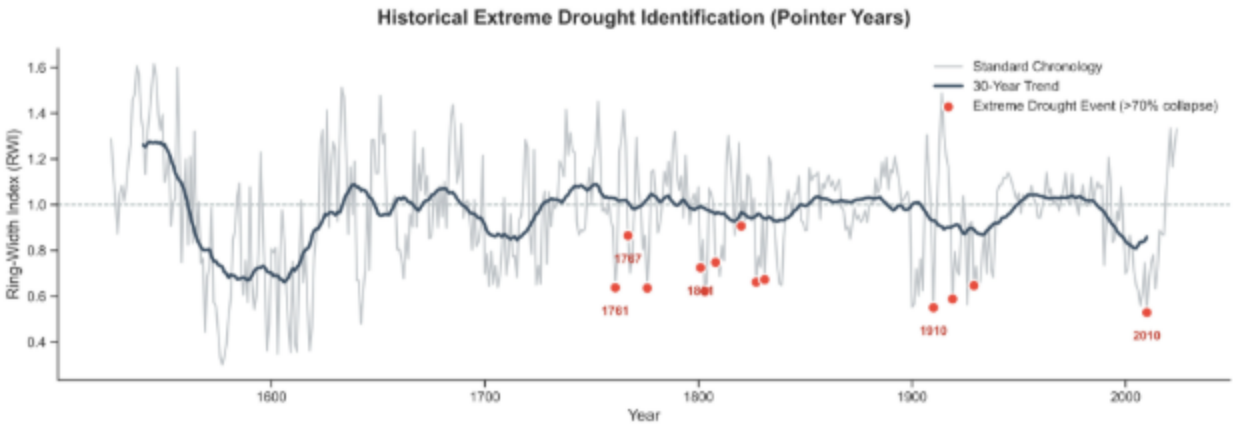


Figure 6

Extreme historical growth-collapse events identified by Pointer Year Analysis. Red filled circles denote years where > 70% of sampled trees exhibited synchronous growth collapse, applied as a single consistent threshold across the chronology. Year labels indicate the most severe events discussed in the text. The grey dashed horizontal line marks the long-term RWI mean; the dark trend line is the 30-year moving average.

Supplementary Files

This is a list of supplementary files associated with this preprint. Click to download.

- SupplementaryCD.docx